Article

Investigation on Crystallization and Magnetic Properties of (Nd, Pr, Ce)$_2$Fe$_{14}$B/α-Fe Nanocomposite Magnets by Microwave Annealing Treatment

Zhanyong Wang [1],* , Changping Shangguan [1], Zemin Wang [1],* , Tianpeng Wang [1], Lianbo Wang [1], Min Liu [1] and Yanli Sui [2]

1   Department of Materials Science and Engineering, Shanghai Institute of Technology, Shanghai 201418, China; harrisguan@126.com (C.S.); wangtianpeng0528@163.com (T.W.); wanglianbo021@hotmail.com (L.W.); liumin110ok@163.com (M.L.)
2   Department Key Laboratory for Advanced Metals and Materials, University of Science and Technology Beijing, Beijing 100083, China; yls@ustb.edu.cn
*   Correspondence: wzy2195@sit.edu.cn (Z.W.); wzm@sit.edu.cn (Z.W.); Tel.: +86-021-6087-3529 (Zhanyong Wang)

Abstract: In the present work, the structures and magnetic properties of (Nd, Pr, Ce) $_2$Fe$_{14}$B/α-Fe nanocomposite magnets were thoroughly investigated. The microwave annealing was applied to achieve a uniform heating effect and uniform grains. Microwave annealing is more favorable to obtain α-Fe phase than conventional annealing, which leads to the enhanced coercivity of hysteresis loops. The coercivity of nanocomposite magnets was 245 kA/m after annealing at 2000 W for 10 min.

Keywords: (Nd; Pr; Ce)$_2$Fe$_{14}$B/α-Fe; nanocomposite magnets; microwave-assisted annealing

1. Introduction

Nd$_2$Fe$_{14}$B/α-Fe nanocomposite magnets have attracted considerable research attention owing to the highest theoretical maximum energy product [1–3]. As previously reported, adjustment of the alloy composition and control of the crystallization process, especially the substitution of the Fe and Nd elements [4–6] was applied to improve the microstructure and properties [7,8]. Many elements (such as Pr, Y, etc.) have been applied to tailor the grain size and the crystallization phase [9–11]. As two effective rare earth elements, Pr and Ce have been widely used to substitute the Fe and Nd elements of Nd$_2$Fe$_{14}$B/α-Fe nanocomposite magnets and adjust their magnetic properties. Pr$_2$Fe$_{14}$B and Ce$_2$Fe$_{14}$B have the same crystal structure as the Nd$_2$Fe$_{14}$B, and the replacement of Ce element to Nd is beneficial to reduce the cost of RE-Fe-B magnets [12]. Nevertheless, the substitution of Ce for Nd deteriorates the magnetic properties because of the formation of Ce$_2$Fe$_{14}$B with low intrinsic magnetic properties [13], so in this research, the addition of Pr element is necessary, because the Pr substitution for the Nd improves the hard magnetic properties of the nanocomposite magnets [14]. The magnetic properties are significantly improved after the substitution of Ce and Pr elements to Nd [15]. Diffusion-processing is the typical method to fabricate high magnetic performance Nd-Pr-Ce-Fe-B sintered magnets [16]. For nanocomposite magnets with Ce and Pr substitution, the uniform and fine microstructure become the critical factor in improving the magnetic properties.

As is well known, the optimization of the annealing process is one of the effective ways to obtain uniform and fine microstructure of nanocomposite magnets [17,18]. The microwave heating process has shown significant advantages against conventional heating procedures in structure controlling. Microwave heating can heat materials to high temperatures with ultra-fast heating rates, short time, and high energy efficiency [19–24]. A higher heating rate favors obtaining uniform and refined grains after the crystallization process [25], enhancing coercivity, and also adjusts the proportion of hard and soft phases.

Thus, the application of microwave annealing may show great benefit for the improvement of magnetic properties of $Nd_2Fe_{14}B/\alpha$-Fe nanocomposite magnets.

The contributions of our research are highlighted as follows: we crystallized amorphous $(Nd, Pr, Ce)_2Fe_{14}B/\alpha$-Fe nanocomposite ribbons by microwave heating treatment and investigated their magnetic properties, which has rarely been reported before.

2. Materials and Methods

2.1. Materials

The ingots with nominal composition $(Nd_{0.525}Pr_{0.175}Ce_{0.3})_9Fe_{64.5}Co_3Cu_{0.5}Ti_1B_{22}$ ribbons were prepared by arc-melting under a high-purity Ar atmosphere. The sizes of small pieces of ingots are 5–7 mm, they were re-melted and spun onto a copper roll, and the wheel speed 22 m/s.

2.2. Methods

To study the effect of microwave-assisted annealing on crystallization, we used a quartz tube with a vacuum of 5×10^{-3} Pa to seal the as-spun ribbons, and apply direct microwaves on ribbons at 650 °C for 10 min under the power of 800, 1500, and 2000 W, respectively. The HAMiLab-V3 microwave furnace (Beijing Yiye Lantian Technology Co., Ltd., Beijing, China) with a frequency of 2.45 GHz is experimental equipment. The $(Nd_{0.525}Pr_{0.175}Ce_{0.3})_9Fe_{64.5}Co_3Cu_{0.5}Ti_1B_{22}$ as-spun ribbons were heated at a rate of 5, 20, and 40 °C/min. We used a differential scanning calorimeter (DSC, (Shanghai Precision Scientific Instrument Co., Ltd., Shanghai, China) to characterize the as-spun ribbons, and X-ray diffraction (XRD) with Cu-Kα radiation to determine the structure of the as-spun and annealed ribbons. A vibrating sample magnetometer (VSM, (YP Magnet Technology Development Co., Ltd.) is used to measure the magnetic properties of the ribbons with a maximum applied magnetic field of 1.8 T.

3. Results and Discussion

3.1. Crystallization Process

The XRD pattern of $(Nd_{0.525}Pr_{0.175}Ce_{0.3})_9Fe_{64.5}Co_3Cu_{0.5}Ti_1B_{22}$ as-spun ribbons is shown in Figure 1. No distinct diffraction peaks were found in the patterns, the broad peak in the interval 35–50 degrees is due to the amorphous phase.
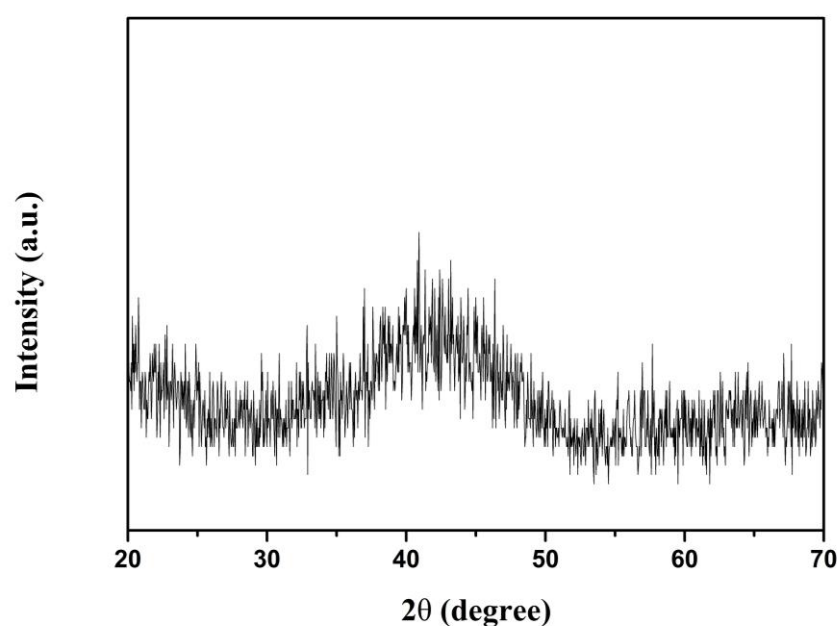
Figure 1. X-ray diffraction pattern of the $(Nd_{0.525}Pr_{0.175}Ce_{0.3})_9Fe_{64.5}Co_3Cu_{0.5}Ti_1B_{22}$ as-spun ribbons.

The DSC curves of the $(Nd_{0.525}Pr_{0.175}Ce_{0.3})_9Fe_{64.5}Co_3Cu_{0.5}Ti_1B_{22}$ as-spun ribbons at a heating rate of 5, 20, and 40 °C/min are shown in Figure 2. Only one exothermic peak is detected, which indicates the synchronized precipitation of soft and hard magnetic phases, and they were formed at the same temperature. The crystallization characteristic temperature increased with the increase of the heating rate due to the hysteresis effect of phase change and the superheat. Moreover, as the heating rate increased, the higher the phase change energy storage per unit time was, the higher the heat released during the phase change was, so the exothermic peak became larger. Activation energy during the crystallization is a crucial parameter of thermal stability for the amorphous alloy, which statistically reflects the average of the activation energy in the crystallization process. The crystallization tendency of the amorphous alloy decreases with the increase of effective activation energy. According to Kissinger equation [26]:

$$In\frac{T^2}{B} = \frac{E}{RT}+C \tag{1}$$

where In is natural logarithm; B is the heating rate; T is the characteristic crystallization temperature (in this study, we select $T = T_p$); E is the crystallization activation energy; R is the molar gas constant; and C is constant. The linear relationship between $\frac{T^2}{B}$ and $\frac{1}{T}$ is shown in Figure 3. The slope values of E/R represent crystallization activation energy, resulting from $E = 121.1$ KJ/mol.
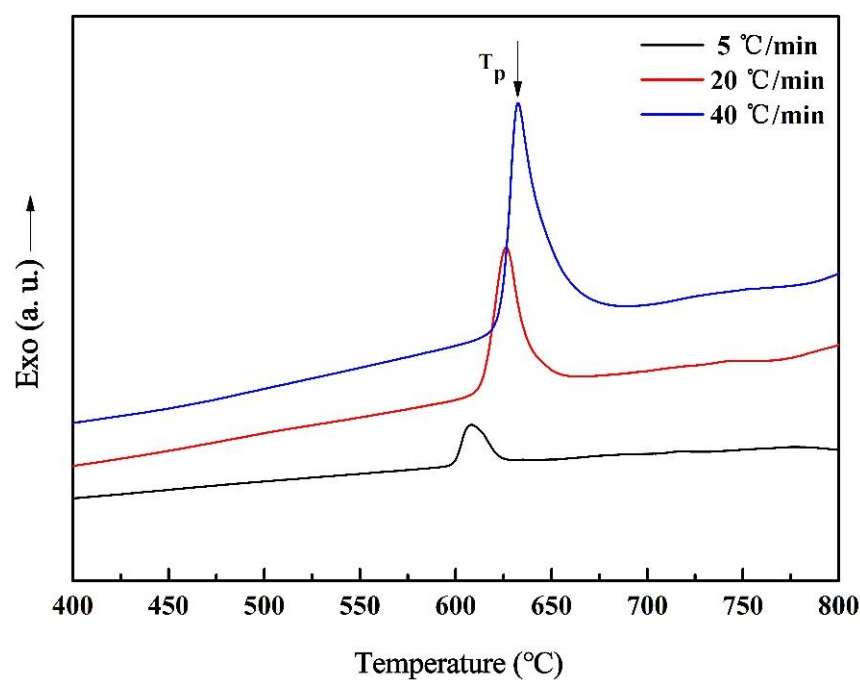
Figure 2. DSC curves of the $(Nd_{0.525}Pr_{0.175}Ce_{0.3})_9Fe_{64.5}Co_3Cu_{0.5}Ti_1B_{22}$ as-spun ribbons.
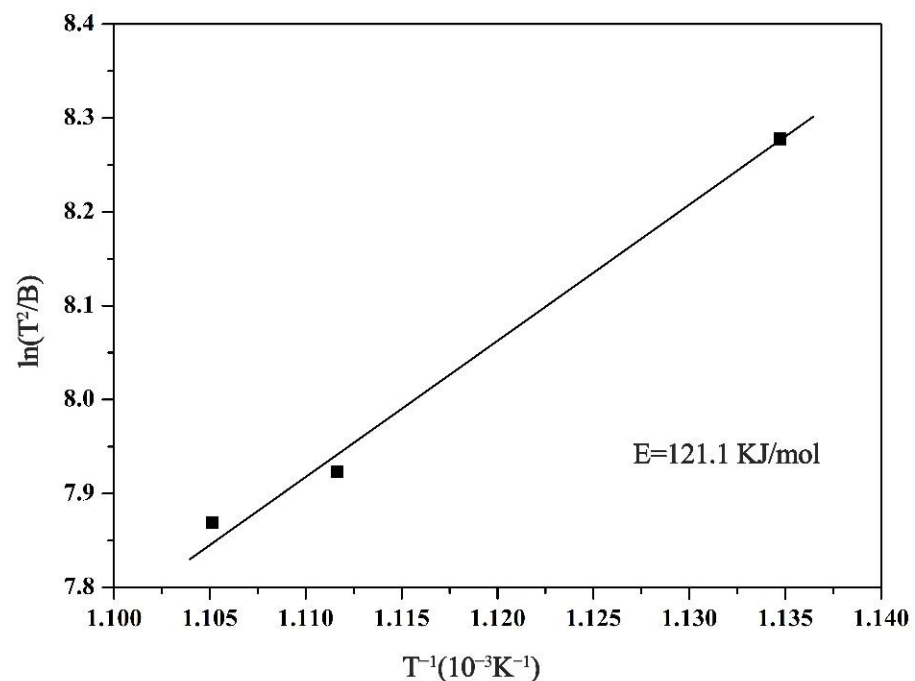
Figure 3. Kissinger curve of the $(Nd_{0.525}Pr_{0.175}Ce_{0.3})_9Fe_{64.5}Co_3Cu_{0.5}Ti_1B_{22}$ as-spun ribbons.

3.2. Comparison of Conventional Annealing and Microwave Annealing

The XRD patterns of the $(Nd_{0.525}Pr_{0.175}Ce_{0.3})_9Fe_{64.5}Co_3Cu_{0.5}Ti_1B_{22}$ ribbons annealed at 650 °C for 10 min under conventional and microwave heating conditions, respectively, are shown in Figure 4. Apart from the diffraction peaks from $(Nd, Pr, Ce)_2Fe_{14}B$ and α-Fe phases, a broad peak locates from 20 degrees to 25 degrees is detected, suggesting the presence of some amorphous phases after conventional annealing treatment. However, the ribbons were annealed by microwave by increasing the microwave power from 800 W to 2000 W, the intensity of the α-Fe peak became significantly stronger than the $(Nd, Pr, Ce)_2Fe_{14}B$ peak. The grain size can be calculated from the line width (FWHM in radian) of XRD [27]. It shows that with the increase of microwave power, the grain size of the α-Fe phase increased greatly; however, the grain size of the $(Nd, Pr, Ce)_2Fe_{14}B$ phase increased slightly, as are shown in Table 1, because microwave annealing treatment promotes the diffusion of elements, accelerates the crystallization rate, and then promotes the growth of grains, especially the α-Fe phase. The average size of grains increases from 11.9 nm in traditional annealing to 40.3 nm in microwave annealing at 2000 W. It explained that the microwave annealing treatment increased the grain size. Moreover, the broad peak completely disappears, presenting the elimination of the residual amorphous phase. The desired microstructural modifications have been achieved in the $(Nd, Pr, Ce)_2Fe_{14}B/\alpha$-Fe samples after microwave annealing for the full range of power. The diffusion rates of the elements were promoted by a microwave field, the proportion of hard and soft magnetic phases were adjusted as well.

Table 1. The average crystallites size of the main phases of the microwave annealed $(Nd_{0.525}Pr_{0.175}Ce_{0.3})_9$ $Fe_{64.5}Co_3Cu_{0.5}Ti_1B_{22}$ ribbons under different power applied.

Power Applied	D (nm)	
	α-Fe	$(Nd, Pr, Ce)_2Fe_{14}B$
conventional	11.9	9.6
800 W	17.7	12.3
1500 W	25.3	12.9
2000 W	41.3	18.6
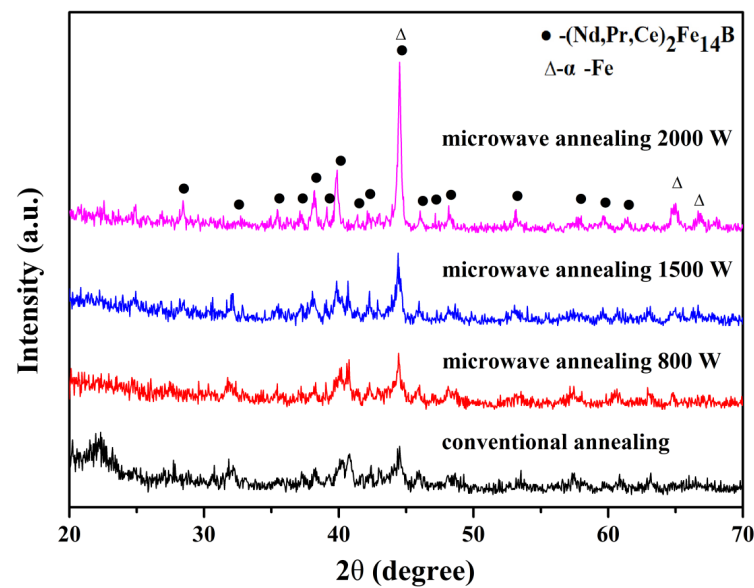
Figure 4. X-ray diffraction patterns of the annealed $(Nd_{0.525}Pr_{0.175}Ce_{0.3})_9Fe_{64.5}Co_3Cu_{0.5}Ti_1B_{22}$ ribbons under different conditions.

The hysteresis loop curves of the $(Nd_{0.525}Pr_{0.175}Ce_{0.3})_9Fe_{64.5}Co_3Cu_{0.5}Ti_1B_{22}$ ribbons annealed at 650 °C for 10 min under conventional heating and microwave heating under different powers are shown in Figure 5. Their hysteresis loops display low magnetic properties. As reported, the $Ce_2Fe_{14}B$ phase presents a lower first-order anisotropy constant than the $Nd_2Fe_{14}B$ phase at room temperature, which induced the decrease of coercivity [28–30]. Even though it is expected that microwave heat treatment will increase the residual magnetization, there is no significant residual magnetic enhancement effect, and there is a weak exchange coupling effect between the soft and hard magnetic phases. The coercivity was enhanced with higher microwave power. It shows that the ribbons' coercivity and remanence magnetic ratio under microwave annealing treatment with a power of 2000 W reaches 245 kA/m and 0.34, which are higher than that of conventional annealing (132 kA/m and 0.26), as are shown in Table 2.
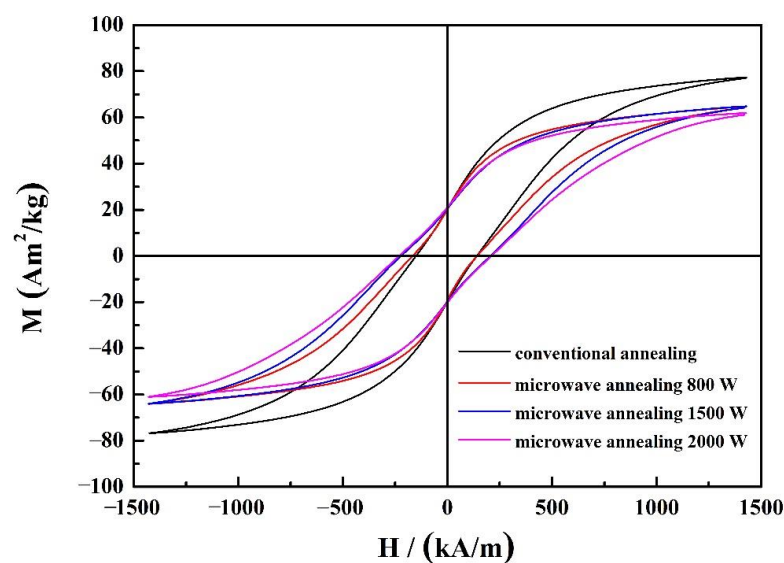
Figure 5. Hysteresis loop curves of the annealed $(Nd_{0.525}Pr_{0.175}Ce_{0.3})_9Fe_{64.5}Co_3Cu_{0.5}Ti_1B_{22}$ ribbons under different conditions.

Table 2. The magnetic properties of the annealed $(Nd_{0.525}Pr_{0.175}Ce_{0.3})_9Fe_{64.5}Co_3Cu_{0.5}Ti_1B_{22}$ ribbons under different annealing conditions.

Annealing Conditions	σ_s (Am²/kg)	σ_r (Am²/kg)	H_c (kA/m)	σ_r/σ_s
conventional	78	20	132	0.26
800 W	65	20	135	0.31
1500 W	65	20	242	0.31
2000 W	61	21	245	0.34

The σ_s is remanence magnetic, σ_r is saturation value of magnetization, H_c is coercivity, and σ_r/σ_s is remanence magnetic ratio.

The X-ray diffraction patterns of the $(Nd_{0.525}Pr_{0.175}Ce_{0.3})_9Fe_{64.5}Co_3Cu_{0.5}Ti_1B_{22}$ ribbons annealed for 5, 10, and 15 min at a microwave power of 2000 W, as are, respectively, shown in Figure 6. With the increase of crystallization time, the intensity of the pattern peaks has an increasing tendency. It shows that the grain size of the α-Fe phase increased greatly; however, the grain size of the $(Nd, Pr, Ce)_2Fe_{14}B$ phase increased slightly, as is shown in Table 3. This is because the elements are difficult to fully diffuse in a short crystallization time, so the grains did not have enough time to grow. When annealing for 5 min, the average grain size of the α-Fe phase is only 26.9 nm. However, when the crystallization time is longer, the elements can fully diffuse, which promotes the grain growth; when annealing for 15 min, the average grain size of the α-Fe phase reached 60.2 nm. It indicated that the crystallization time affected the grain size and adjustment of the percentage of soft and hard magnetic phases.
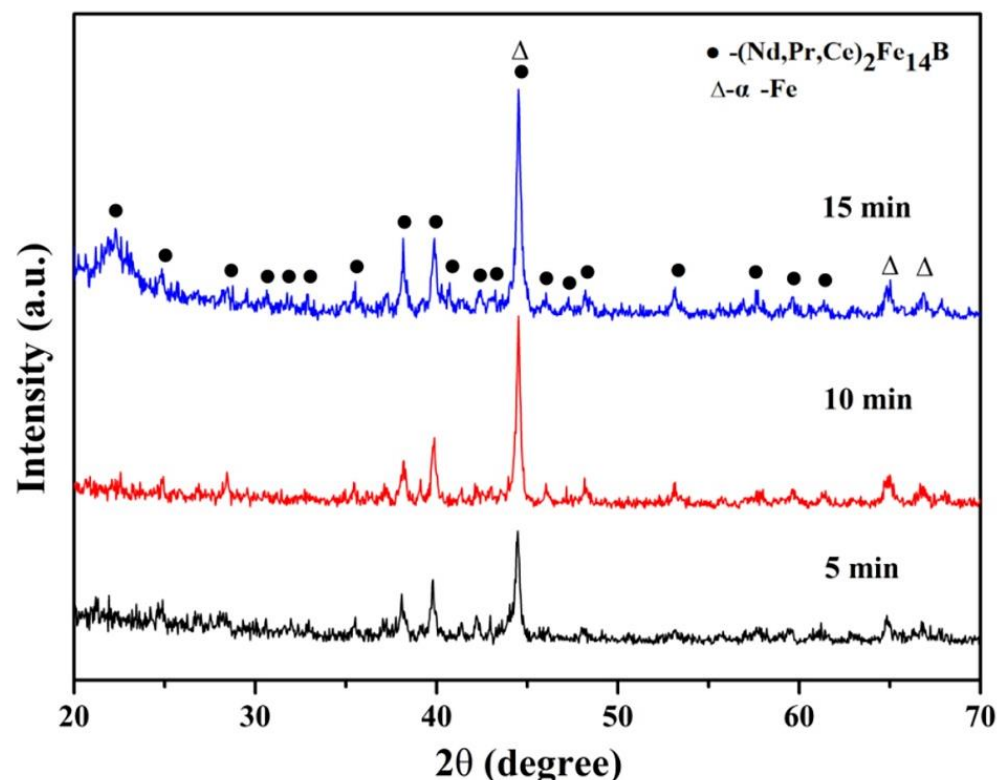
Figure 6. X-ray diffraction patterns of the microwave annealed $(Nd_{0.525}Pr_{0.175}Ce_{0.3})_9Fe_{64.5}Co_3Cu_{0.5}Ti_1B_{22}$ ribbons for different time.

Table 3. The average crystallites size of the main phases of the microwave annealed $(Nd_{0.525}Pr_{0.175}Ce_{0.3})_9Fe_{64.5}Co_3Cu_{0.5}Ti_1B_{22}$ ribbons for a different time.

Annealing Time (min)	D (nm)	
	α-Fe	$(Nd, Pr, Ce)_2Fe_{14}B$
5	26.9	11.7
10	41.3	18.6
15	60.2	22.4

The hysteresis loop curves of the $(Nd_{0.525}Pr_{0.175}Ce_{0.3})_9Fe_{64.5}Co_3Cu_{0.5}Ti_1B_{22}$ ribbons annealed for 5, 10, and 15 min at a microwave power of 2000 W, are, respectively, shown in Figure 7. It shows that annealing under the microwave power of 2000 W for 10 min could obtain a higher coercivity and residual magnetization, 245 kA/m and 21 Am^2/kg, as are, respectively, shown in Table 4. There is no significant residual magnetic enhancement effect, and there is a weak exchange coupling effect between the soft and hard magnetic phases annealing under the microwave power of 2000 W for 10 min. The coercivity and remanent magnetic ratio could be enhanced under appropriate microwave annealing process.
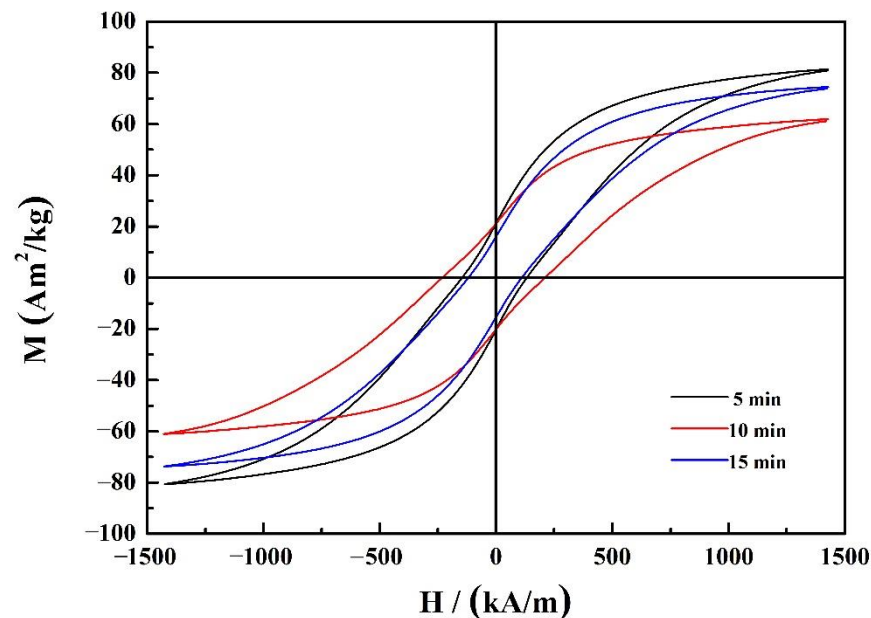
Figure 7. Hysteresis loop curves of the microwave annealed $(Nd_{0.525}Pr_{0.175}Ce_{0.3})_9$ $Fe_{64.5}Co_3Cu_{0.5}Ti_1B_{22}$ ribbons for a different time.

Table 4. The magnetic properties of the annealed $(Nd_{0.525}Pr_{0.175}Ce_{0.3})_9Fe_{64.5}Co_3Cu_{0.5}Ti_1B_{22}$ ribbons for a different time.

Annealing Times (min)	σ_s (Am^2/kg)	σ_r (Am^2/kg)	H_c (kA/m)	σ_r/σ_s
5	81	21	127	0.27
10	61	23	245	0.38
15	74	18	119	0.24

The σ_s is remanence magnetic, σ_r is saturation value of magnetization, H_c is coercivity, and σ_r/σ_s is remanence magnetic ratio.

4. Conclusions

This study investigated the crystallization and magnetic properties of $(Nd, Pr, Ce)_2Fe_{14}B/$ α-Fe nanocomposite magnets through microwave annealing treatment. The results of the

experiment indicate that compared with traditional annealing, even though microwave annealing slightly reduces the magnetic saturation strength of the magnet, it increases the coercivity and remanence ratio of $(Nd, Pr, Ce)_2Fe_{14}B/\alpha$-Fe nanocomposite magnets. Coercivity and remanence ratio up to 245 kA/m and 0.38 for $(Nd_{0.525}Pr_{0.175}Ce_{0.3})_9Fe_{64.5}Co_3Cu_{0.5}Ti_1B_{22}$ ribbons were obtained after annealed at microwave field with 2000 W for 10 min.

Author Contributions: Conceptualization, Z.W. (Zhanyong Wang); methodology, C.S., M.L., Y.S. and T.W.; investigation, C.S., L.W., Z.W. (Zemin Wang) and T.W.; data analysis, C.S., L.W, Y.S. and T.W.; writing—original draft preparation, C.S. and T.W.; writing—review and editing, T.W., Z.W. (Zemin Wang), L.W. and M.L.; funding acquisition, M.L., Y.S. and Z.W. (Zhanyong Wang); supervision, Z.W. (Zemin Wang), Z.W. (Zhanyong Wang). All authors have read and agreed to the published version of the manuscript.

Institutional Review Board Statement: Not applicable.

Informed Consent Statement: Not applicable.

Data Availability Statement: No new data were created or analyzed in this study. Data sharing is not applicable to this article.

Conflicts of Interest: The authors declare no conflict of interest.

References

1. Ryo, H.S.; Hu, L.X.; Kim, J.G. Micromagnetic study for magnetic properties of exchange coupled nanocomposite magnetic systems with $Nd_2Fe_{14}B$ grains embedded in α-Fe matrix. *J. Magn. Magn. Mater.* **2017**, *426*, 46–52. [CrossRef]
2. Yu, X.Q.; Yue, M.; Liu, W.Q.; Li, Z.; Zhu, M.G.; Dong, S.Z.J. Structure and intrinsic magnetic properties of $MM_2Fe_{14}B$ (MM = La, Ce, Pr, Nd) alloys. *Rare Earths* **2016**, *34*, 614–617. [CrossRef]
3. Li, H.L.; Li, W.; Zhang, Y.M.; Gunderov, D.V.; Zhang, X.Y. Phase evolution, microstructure, and magnetic properties of bulk Alpha-Fe/$Nd_2Fe_{14}B$ nanocomposite magnets prepared by severe plastic deformation and thermal annealing. *J. Alloys Compd.* **2015**, *651*, 434–439. [CrossRef]
4. Wang, Z.Y.; Liu, W.Q.; Zhou, B.X.; Ni, J.S.; Xu, H.; Li, Q. Microstructural characteristics of $Nd_2Fe_{14}B/\alpha$-Fe nanocomposite ribbons bearing Nb element. *Rare Metals* **2008**, *27*, 299–302. [CrossRef]
5. Wang, H.Y.; Zhao, F.A.; Chen, N.X.; Liu, G. Theoretical investigation on the phase stability of $Nd_2Fe_{14}B$ and site preference of V, Cr, Mn, Zr, and Nb. *J. Magn. Magn. Mater.* **2005**, *295*, 219–229. [CrossRef]
6. Yamamoto, H.; Takahashi, K.; Hamano, R. Magnetic properties of low Rare-Earth composition Pr–Fe–Co–Ti–Nb–B system exchange-spring magnets. *J. Alloys Compd.* **2006**, *408*, 1417–1421. [CrossRef]
7. Hussain, M.; Zhao, L.Z.; Zhang, C.; Jiao, D.L.; Zhong, X.C.; Liu, Z.W. Composition-Dependent magnetic properties of melt-spun La or/and Ce substituted nanocomposite NdFeB alloys. *Phys. B* **2016**, *483*, 69–74. [CrossRef]
8. Wang, X.C.; Zhu, M.G.; Li, W.; Zheng, L.Y.; Guo, Z.H.; Du, X.; Du, A.; Wang, X.C.; Zhu, M.G. Effects of the ingot phase transition on microstructure and magnetic properties of CeNdFeB Melt-Spun ribbons. *Phys. B* **2015**, *476*, 255–258. [CrossRef]
9. Yao, Q.R.; Shen, Y.H.; Yang, P.C.; Zhou, H.Y.; Rao, G.H.; Deng, J.Q.; Wang, Z.M.; Zhong, Y. Crystal structure and phase relations of $Pr_2Fe_{14}B$-$La_2Fe_{14}B$ system. *J. Rare Earths* **2016**, *34*, 1121–1125. [CrossRef]
10. Zhan, Y.Y.; Pan, J.; Jiang, X.L.; Liu, X.C.; Dong, Y.R.; Xiao, X.Y. Microstructure evolution and magnetic properties of the Nd9Fe81-xTi4C2Nb4Bx (x=11, 13, 15) bulk magnets prepared by copper mold suction casting. *J. Rare Earths* **2015**, *33*, 1081–1086. [CrossRef]
11. Susner, M.A.; Conner, B.S.; Saparov, B.I.; McGuire, M.A.; Crumlin, E.J.; Veith, G.M.; Huibo Cao, H.B.; Shanavas, K.V.; Parker, D.S.; Zhang, Y.J. Flux growth and characterization of Ce-Substituted $Nd_2Fe_{14}B$ single crystals. *J. Magn. Magn. Mater.* **2017**, *434*, 1–9. [CrossRef]
12. Jiang, Q.; Zhong, Z. Research and development of Ce-Containing $Nd_2Fe_{14}B$-type alloys and permanent magnetic materials. *J. Mater. Sci. Technol.* **2017**, *33*, 1087–1096. [CrossRef]
13. Chen, Z.; Lim, Y.K.; Brown, D. Substitution of Ce for (Nd, Pr) in Melt-Spun (Nd, Pr)–Fe–B Powders. *IEEE Trans. Magn.* **2015**, *51*, 1–4. [CrossRef]
14. Zhang, W.-Y.; Zhang, S.-Y.; Yan, A.-R.; Zhang, H.-W.; Shen, B.-G. Effect of the substitution of Pr for Nd on microstructure and magnetic properties of nanocomposite $Nd_2Fe_{14}B/\alpha$-Fe magnets. *J. Magn. Magn. Mater.* **2001**, *225*, 389–393. [CrossRef]
15. Wei, T.; Guozhi, X. Effects of the Annealing Process on the Microwave Properties of Quenched Nd-Fe-B Alloys. In Proceedings of the 2nd International Conference on Intelligent Materials and Mechatronics(IMM 2015) and 2nd International Conference on Solar Energy Materials and Energy Engeering(SEMEE 2015), Hong Kong, China, 29 October 2015; pp. 143–147.

16. Zhang, Y.J.; Ma, T.Y.; Yan, M.; Jin, J.Y.; Liu, X.L.; Xu, F.; Miao, X.F.; Liu, X.L. Squareness factors of demagnetization curves for multi-main-phase Nd-Ce-Fe-B magnets with different Ce contents. *J. Magn. Magn. Mater.* **2019**, *487*. [CrossRef]

17. Zhang, Y.F.; Han, J.Z.; Liu, S.Q.; Wan, F.M.; Tian, H.D.; Zhang, X.D.; Wang, C.S.; Yang, J.B.; Yang, Y.C. Coercivity enhancement by grain refinement for anisotropic $Nd_2Fe_{14}B$-type magnetic powders. *Scr. Mater.* **2016**, *110*, 57–60. [CrossRef]

18. Oghbaei, M.; Mirzaee, O. Microwave versus conventional sintering: A review of fundamentals, advantages, and applications. *J. Alloys Compd.* **2010**, *494*, 175–189. [CrossRef]

19. Xu, R.; He, J.; Li, W.; Paine, D.C. Performance enhancement of amorphous Indium-Zinc-Oxide Thin-Film transistors by microwave annealing. *Appl. Surf. Sci.* **2015**, *357*, 1915–1919. [CrossRef]

20. Cichoň, S.; Machác, P.; Fekete, L.; Lapcák, L. Direct microwave annealing of SiC substrate for rapid synthesis of quality epitaxial graphene. *Carbon* **2016**, *98*, 441–448. [CrossRef]

21. Mirzaei, A.; Neri, G. Microwave-assisted synthesis of metal oxide nanostructures for gas sensing application: A review. *Sens. Actuat B Chem.* **2016**, *237*, 749–775. [CrossRef]

22. Swaminathan, V.; Deheri, P.K.; Bhame, S.D.; Ramanujan, R.V. Novel microwave assisted chemical synthesis of $Nd_2Fe_{14}B$ hard magnetic nanoparticles. *Nanoscale* **2013**, *5*, 2718–2725. [CrossRef]

23. Sun, Y.; Jin, M.; Wang, Z.Y.; Jiang, H. Microwave Sintering of High Performance Strontium Ferrite Magnets and Their Magnetic Properties. *J. Synth. Cryst.* **2013**, *42*, 751–755.

24. Gjoka, M.; Neil, D.; Hadjipanayis, G.; Niarchos, D.G. Experimental Proof of Microwave Sintering of Nd–Fe–B Powders Toward Fabrication of Permanent Magnets. *IEEE Trans. Magn.* **2014**, *50*, 1–4. [CrossRef]

25. Wang, T.P.; Tian, T.; Ding, S.; Wang, Z.Y.; Ni, Q.X.; Zhou, D.; Dong, G.L.; Sui, Y.L.; Jin, M.L. Effects of Microwave-Assisted Annealing on the Structure and Magnetic Properties of $(Nd_{0.75}Pr_{0.25})_9Fe_{72}Ti_1Zr_3Mn_xMo_{4-x}B_{10.5}C_{0.5}$ Amorphous Ribbons. *J. Supercond. Nov. Magn.* **2018**, *31*, 2241–2246. [CrossRef]

26. Blaine, R.L.; Kissinger, H.E. Homer Kissinger, and the Kissinger equation. *Thermochim. Acta.* **2012**, *540*, 1–6. [CrossRef]

27. Zhou, X.D.; Huebner, W. Size-induced lattice relaxation in $CeO2$ nanoparticles. *Appl. Phys. Lett.* **2001**, *79*, 3512. [CrossRef]

28. Hirosawa, S.; Matsuura, Y.; Yamamoto, H.; Fujimura, S.; Sagawa, M.; Yamauchi, H. Single crystal measurements of anisotropy constants of $R_2Fe_{14}B$ (R = y, Ce, Pr, Nd, Gd, Tb, Dy and Ho). *Jpn. J. Appl. Phys.* **1985**, *24*, 803–805. [CrossRef]

29. Herbst, J.F.; Hector, L.G. A computational quest for $Nd_2Fe_{14}B$-type Ce and Nd phases. *J. Alloys Compd.* **2017**, *693*, 238–244. [CrossRef]

30. Yang, M.N.; Wang, H.; Hu, Y.F.; Yang, L.Y.M.; Maclennan, A.; Yang, B. Increased coercivity for Nd-Fe-B melt spun ribbons with 20 at.% Ce addition: The role of compositional fluctuation and Ce valence state. *J. Alloys Compd.* **2017**, *710*, 519–527. [CrossRef]